

# Optical Properties of Tricarboxylic Acid-Derived Carbon Dots

Aleksandra Tomskaya,\* Igor P. Asanov, Irina Yushina, Mariana I. Rakhmanova, and Svetlana Smagulova

Cite This: *ACS Omega* 2022, 7, 44093–44102

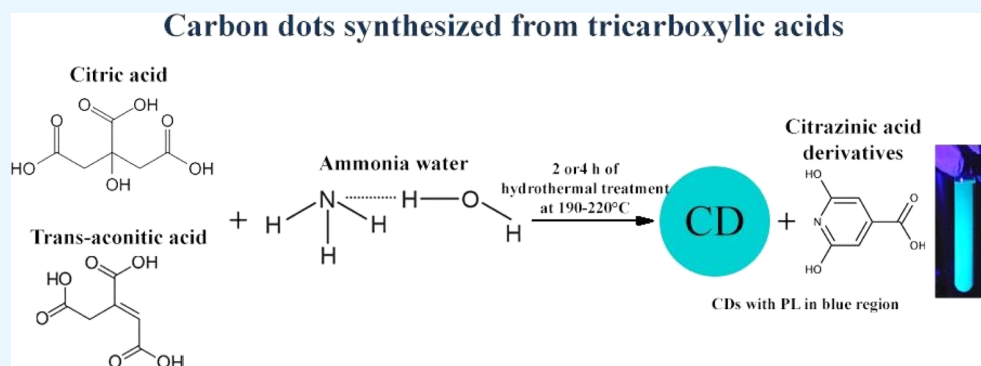
Read Online

ACCESS |

Metrics &amp; More

Article Recommendations

Supporting Information



**ABSTRACT:** Herein, we report the characterization of two types of luminescent carbon dots (CDs) synthesized by the hydrothermal treatment of citric acid and *trans*-aconitic acid by using ammonia solution as a nitrogen dopant. The lateral size range of nanoparticles for CDs lies in the range of 3–15 nm. The intense blue photoluminescence (PL) was emitted by the CDs at around 409–435 nm under the excitation of 320 nm. The PL quantum yield of the synthesized CDs ranged from 26.4 to 51%. Our results of the structural and optical properties of CDs imply that molecular fluorophores are an important part of the structure; in particular, the main contribution to the PL is carried by the fluorophores based on citrazinic acid derivatives, which formed during the synthesis of CDs.

## 1. INTRODUCTION

Carbon dots (CDs), as a new type of carbon material of less than 20 nm in size, have drawn attention due to their unique optical properties, such as photoluminescence (PL), photo-induced electron transfer and electrochemiluminescence.<sup>1,2</sup> CDs have potential as a substitute for toxic metal-based quantum dots because of their robust chemical inertness, biocompatibility, simple and inexpensive preparation, low toxicity, and abundance of raw material in nature.<sup>3,4</sup> CDs can find application in areas such as drug delivery, medical diagnosis, two-photon fluorescence imaging, fluorescent ink, detection of metal ions, and catalysis.<sup>5–8</sup> In this connection, several approaches, with a wide variety of synthesis methods and raw precursors used, have been developed to prepare fluorescent CDs in the past 15 years. Generally, these methods for synthesizing CDs are categorized into “top-down” (cutting from different preformed carbon structures) and “bottom-up” (starting with molecular precursors) approaches.<sup>9</sup> Compared to “top-down” methods, the “bottom-up” methods provide easy introduction of heteroatoms into CDs during synthesis, which could significantly affect the properties of the resulting CDs.

CDs synthesized by carbonization of citric acid (CA) are the most interesting in terms of photoluminescent properties.<sup>9,10</sup> Various studies have been devoted to increasing the PL

quantum yield (QY) of these CDs from 10 to 90% by attaching to the CDs of various surface-passivating agents based on amines: ammonia solution, ethylenediamine, cysteine, ethanolamine, and so forth.<sup>9–11</sup> By atomic doping CDs with other heteroatoms, it is possible to adjust their compositions and structures. The N doping of CDs is the most studied due to its efficient and simple one-step strategy, numerous alternative compounds, and large-scale fabrication.<sup>12</sup> We report the synthesis of various N-doped CDs from tricarboxylic acids and ammonia solution by the hydrothermal reaction: CDs from CA and ammonia solution synthesized during 2 (C2-CDs) and 4 (C4-CDs) hours, and CDs from *trans*-aconitic acid (TA) and ammonia solution synthesized during 2 (T2-CDs) and 4 (T4-CDs) hours. We previously reported about the synthesis of CDs from CA and TA.<sup>13</sup> The current study compared in depth the CA- and TA-synthesized CDs with different synthesis times. It is interesting to compare the structural and optical properties of CDs with another

**Received:** August 26, 2022**Accepted:** November 4, 2022**Published:** November 22, 2022

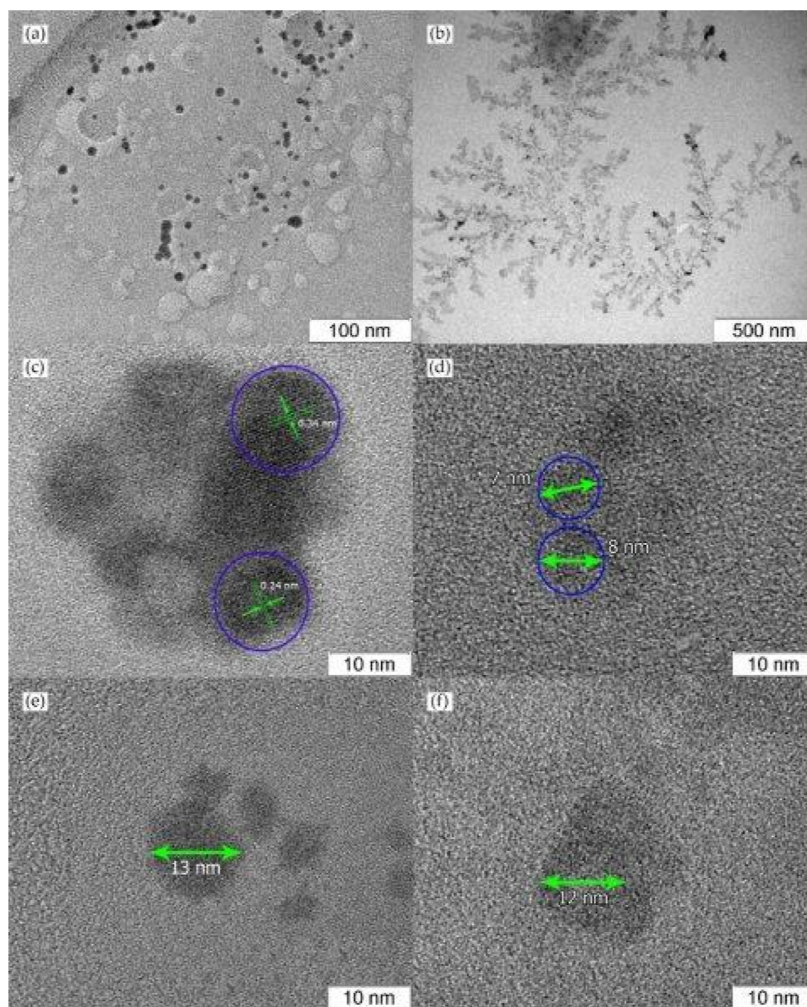


**Figure 1.** TEM images of CD solutions (a) C4-CDs at a scale of 100 nm, (b) T4-CDs at a scale of 500 nm, (c) C4-CDs at a scale of 10 nm, (d) T4-CDs at a scale of 10 nm, (e) C2-CDs at a scale of 10 nm, and (f) T2-CDs at a scale of 10 nm.

tricarboxylic precursor because there are several studies on the synthesis of CDs from CA with high PL QY.<sup>14,15</sup> The ammonia solution was chosen as the nitrogen precursor because an ammonia solution is a base and the source of nitrogen without other atomic impurities. Using CA and TA as precursors, the formation of CDs has been attributed to their carbonization. Carbonization is a complex process in which many reactions occur concurrently, such as dehydration, dehydrogenation, condensation, hydrogen transfer, and isomerization.<sup>16</sup> The dehydrating rate depends on the number of available OH groups.<sup>17</sup> Based on the molecular structures of CA and NH<sub>4</sub>OH, CA has one OH group and three COOH groups, while NH<sub>4</sub>OH has one OH group. Under the heating, the intermolecular and/or intramolecular dehydration reaction should occur in them. However, the dehydration reaction between the OH groups was more favorable than the one between COOH and OH groups in our experiment. Dehydration of two OH groups leads to the formation of C–O–C bonds between two CA molecules or C–N–C between two CA molecules and one NH<sub>4</sub>OH molecule. After that, the processes of condensation and isomerization are as follows, which lead to the formation of CDs.

## 2. MATERIALS

**2.1. Materials.** CA, TA, and ammonia solution (30%) were purchased from OAO “Reaktiv” (JSC, Novosibirsk, Russia). Dialysis bags were purchased from “Rosmedbio” (St. Petersburg, Russia). Silica solid phase extraction (SPE) cartridges were purchased from Dongguan Sainsar Silicone Product Co., Ltd (China). The chemicals were analytically pure and were used in the form in which they were obtained.

**2.2. Synthesis of N-Doped CDs.** For the synthesis of C2-CDs, CA was used as a carbon precursor and ammonia solution was used as a nitrogen precursor. 1.08 g of CA powder (C<sub>6</sub>H<sub>8</sub>O<sub>7</sub>) was dissolved in a mixture of deionized water (18 mL) and ammonia solution (3.5 mL). The solution was transferred to a 25 mL capacity autoclave without further agitation. The Teflon-lined autoclave containing a solution was placed in a drying oven and held for 2 h at a temperature of 190° C (1 MPa). The resulting solution with a total concentration of 0.0357 mg mL<sup>-1</sup> contained C2-CDs and other synthesis products. The solution was dialyzed to isolate pure C2-CDs (1000 Da, 8 h) and filtered through a filtration membrane with a pore size of 100 nm. After that, the solution was filtered through silica SPE cartridges with a pore size of 20 nm to sort C2-CD nanoparticles by size. The final water suspension of C2-CDs had a light-yellow color. The

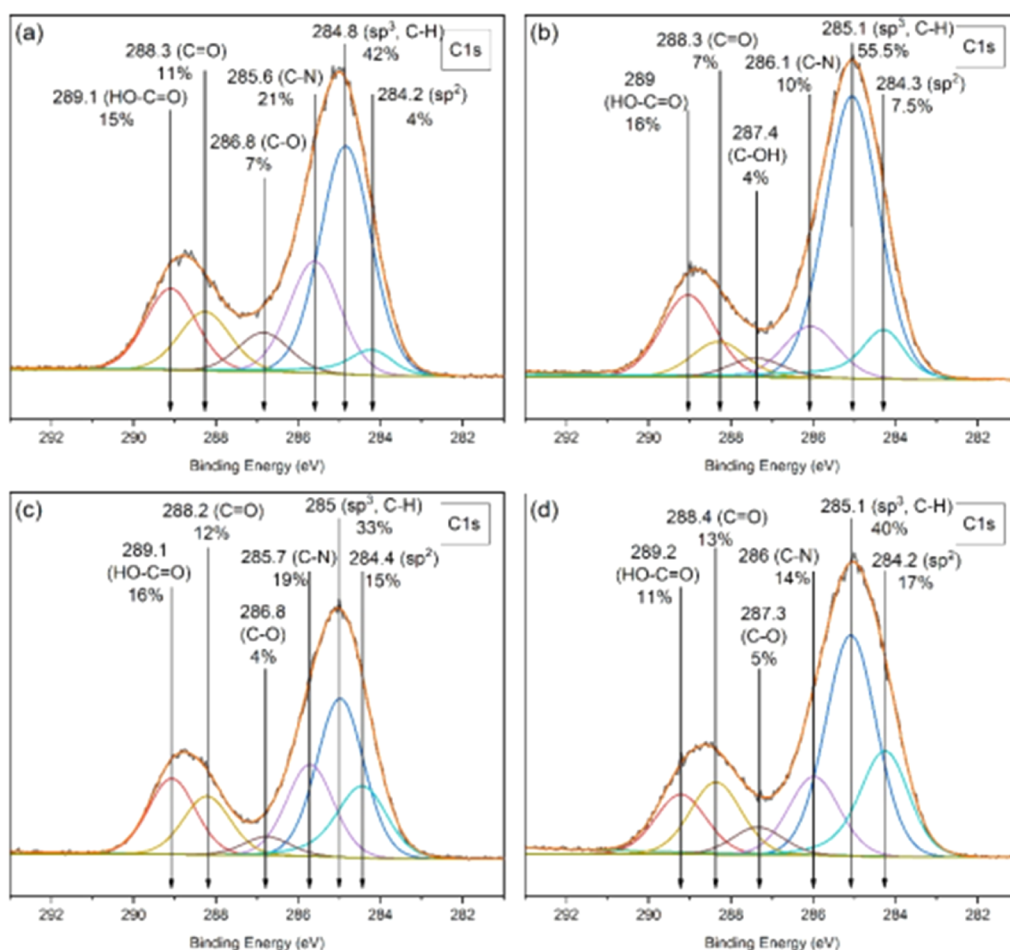


**Figure 2.** C 1s spectra of samples (a) C2-CDs, (b) C4-CDs, (c) T2-CDs, and (d) T4-CDs.

concentration of dry matter in the final solution was 0.006 mg mL<sup>-1</sup>.

Synthesis of C4-CDs was carried out by the same procedure as for sample C2-CDs, except that the solution was placed in a drying oven and held for 4 h at a temperature of 190 °C.

Synthesis of T2-CDs was carried out by the same procedure as for sample C2-CDs, except that *trans*-aconitic acid powder (0.98 g of C<sub>6</sub>H<sub>6</sub>O<sub>6</sub>) was used as the carbon precursor and the solution was placed in a drying oven and held for 2 h at a temperature of 220 °C.

Synthesis of T4-CDs was carried out by the same procedure as for sample T2-CDs, except that the solution was placed in a drying oven and held for 4 h at a temperature of 220 °C.

**2.3. Characterization.** Transmission electron microscopy (TEM) images were made on a JEOL-2010 microscope. The X-ray photoelectron spectroscopy (XPS) measurements of dried CDs were performed on a SPECS photoelectron spectrometer (Berlin, Germany) using a PHOI-BOS-150-MCD-9 hemispherical analyzer and FOCUS-500 X-ray monochromator (AlK $\alpha$  radiation,  $h\nu = 1486.74$  eV, 200 W). The Fourier transform infrared (FT-IR) spectroscopy spectra were recorded with a PerkinElmer Spectrum Two spectrophotometer. Absorption spectra were recorded on a Shimadzu 3101 PC UV/VIS/NIR spectrometer. Emission spectra and luminescence decays were recorded using a Fluorolog 3 spectrometer (Horiba Jobin Yvon) with a cooled PC177CE-010 photon detection module equipped with an R2658 photomultiplier. The exciting slit and the emission slit were

both 2 nm. The absolute values of PL QY were measured using a Fluorolog 3 Quanta-phi device.

### 3. RESULTS

The four kinds of CDs studied here (denoted as C2-CDs, C4-CDs, T2-CDs, and T4-CDs) were synthesized by reactions of ammonia solution with two different carbon-containing precursors (namely, CA and TA) for 2 and 4 h, respectively. TEM images reveal that C2-CDs and C4-CDs are monodisperse nanoparticles of near spherical morphology (Figure 1a,c,e). The growth dynamics of the lateral sizes of CDs with the increase in synthesis time were not observed because all CDs were filtered through silica gel with a pore size of 20 nm. However, the sample C2-CDs contained a larger number of particles up to 15 nm in size in contrast with C4-CDs. TEM images of C4-CDs show lattice fringes with interplanar spacings of  $\sim 0.24$  and  $\sim 0.34$  nm, which are close to the (100) and (002) diffraction facets of graphite carbon, respectively (Figure 1c).<sup>18–20</sup> Further TEM results indicate that the T2-CDs and T4-CDs aggregate into tree-like structures during drying (Figure 1b). The resulting TEM images are not of high quality due to the low electron contrast between the T2-CDs (also for T4-CDs) and the carbon-coated TEM grids. Because of that, the lateral sizes of T2-CDs and T4-CDs are roughly in the range of  $\sim 7$ –12 nm (Figure 1d,f). The size range of particles for all CDs lies in the range of 3–15 nm, and the lateral size distributions of samples are shown in Figure S1 (see Supporting Information, Figure S1). The

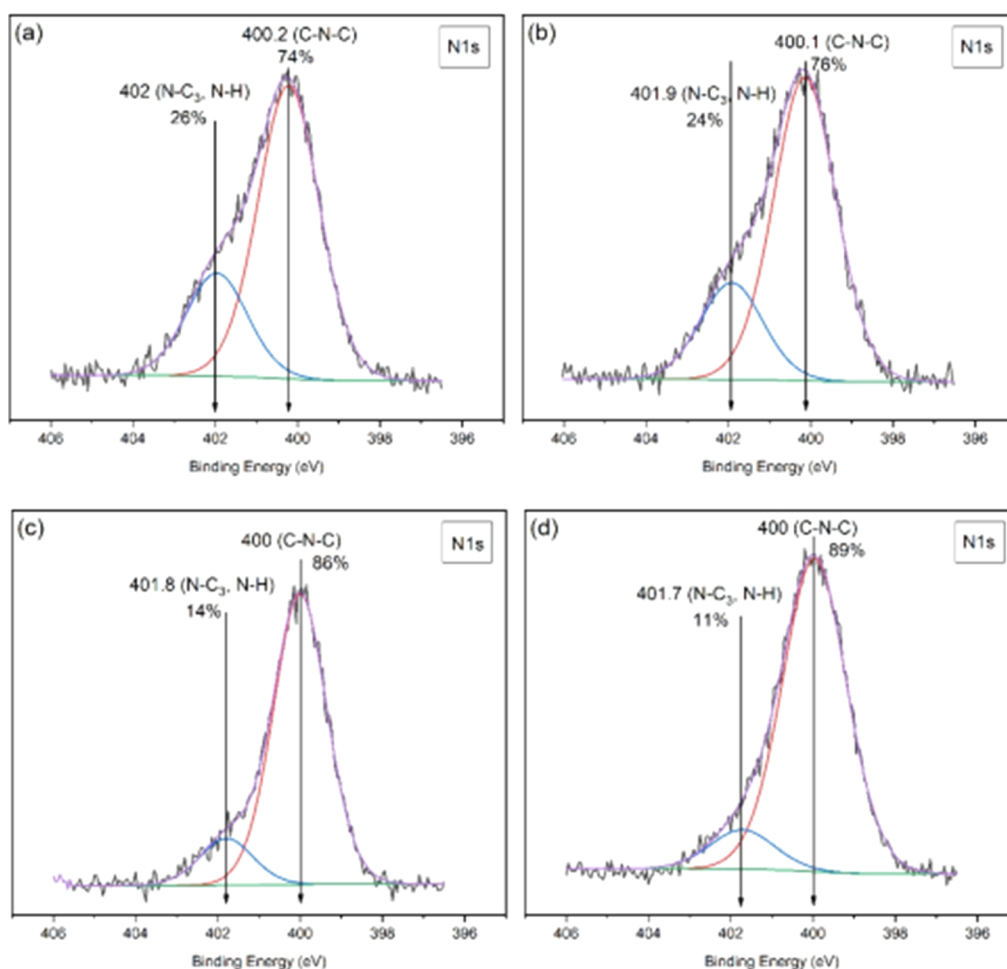


**Figure 3.** N 1s spectra of samples (a) C2-CDs, (b) C4-CDs, (c) T2-CDs, and (d) T4-CDs.

average lateral diameters are 11.7, 13.4, 10.1, and 12.1 for C2-CDs, C4-CDs, T2-CDs, and T4-CDs, respectively.

To investigate the relationship between the PL behavior and the structure of CDs, we applied XPS and FT-IR instruments to determine the chemical bonds and compositions in C2-CDs, C4-CDs, T2-CDs, and T4-CDs.

The XPS survey spectra of all samples are shown in Figure S2 (see Supporting Information, Figure S2). XPS spectra indicate that all CDs contain mainly of carbon, nitrogen, and oxygen bonds (Figure 2). The C/N/O ratio based on the XPS peak are as corrected for element sensitivity was 60:7:33 for C2-CDs, 65:7:28 for C4-CDs, 62:7:31 for T2-CDs, and 65:7:28 for T4-CDs. These results indicate the successful doping of N heteroatoms into CDs. The C 1s spectra of all CDs in Figure 2 demonstrate the existence of bulk  $sp^3$  carbon/C-H (284.8–285.1 eV), surface  $sp^2$  carbon (284.2–284.4 eV), C-N (285.6–286 eV), C-O (286.8–287.3 eV), C=O (288.2–288.4 eV), and HO-C=O (289.1–289.2 eV). The characteristic peak C-C  $sp^2$  suggests that the graphite structure should be contained in the obtained CDs. The presence of peaks C-O, C=O, and HO-C=O indicates that obtained CDs have various polar groups including hydroxyl and carboxyl.<sup>21</sup> N 1s spectra of all CDs (Figure 3) mainly consist of two peaks of pyrrole/pyridone N (C-N-C) (400–400.2 eV) and graphitic N [N-(C)<sub>3</sub>/N-H] (401.7–402 eV).<sup>22,23</sup> The intensity of the pyrrole/pyridone N (C-N-C) peak increases slightly with the increase in synthesis time: the

peak areas are 74 and 76% for C2-CDs and C4-CDs (Figure 3a,b), and 86 and 89% for T2-CDs and T4-CDs, respectively (Figure 3c,d). The O 1s spectra of all CDs in Figure 4 demonstrate the existence of peaks of C=O (531.4–531.8 eV), O=C-OH (532–532.3 eV), C-O (533–533.5 eV), and O-H (533.3–534.1 eV). The O 1s spectrum of C2-CDs has a water peak at 533.9 eV due to insufficient drying of the sample (Figure 4a).

FT-IR spectra in Figure 5a,b illustrate that all CDs are composed of incompletely carbonized CA and TA due to the absorption of stretching vibrations of C=C bonds in isolated C  $sp^2$  domains at 1680–1610  $cm^{-1}$ , in conjugated with C=O groups (1708 and 1776  $cm^{-1}$ ).<sup>23–25</sup> Additionally, FT-IR spectra of all the CDs shows broad absorption bands of stretching vibrations N-H/O-H at 3209–3309  $cm^{-1}$ , C-H at 2928  $cm^{-1}$ , C-N at 1400–1423  $cm^{-1}$ , and carboxylate COO- at 1420  $cm^{-1}$  and a narrow absorption band of bending vibration of N-H at 1553–1565  $cm^{-1}$ .<sup>25,26</sup>

Two characteristic peaks at 1650–1658 and 1553–1565  $cm^{-1}$ , which are consistent with amide I (C=O) and amide II (N-H) vibrations, respectively, indicate the existence of the -OCNH- linker (Figure 5b).<sup>26,27</sup> FT-IR spectra of the samples C4-CDs and T4-CDs show asymmetric stretching vibrations of C-NH-C at 1106–1152  $cm^{-1}$ .<sup>28</sup> Also, it can be seen from the FT-IR spectra that the intensity of the stretching vibrations C=C ( $sp^2$ ) at 1680–1610  $cm^{-1}$  increases for C4-CDs relative to C2-CDs, which is explained by an increase of

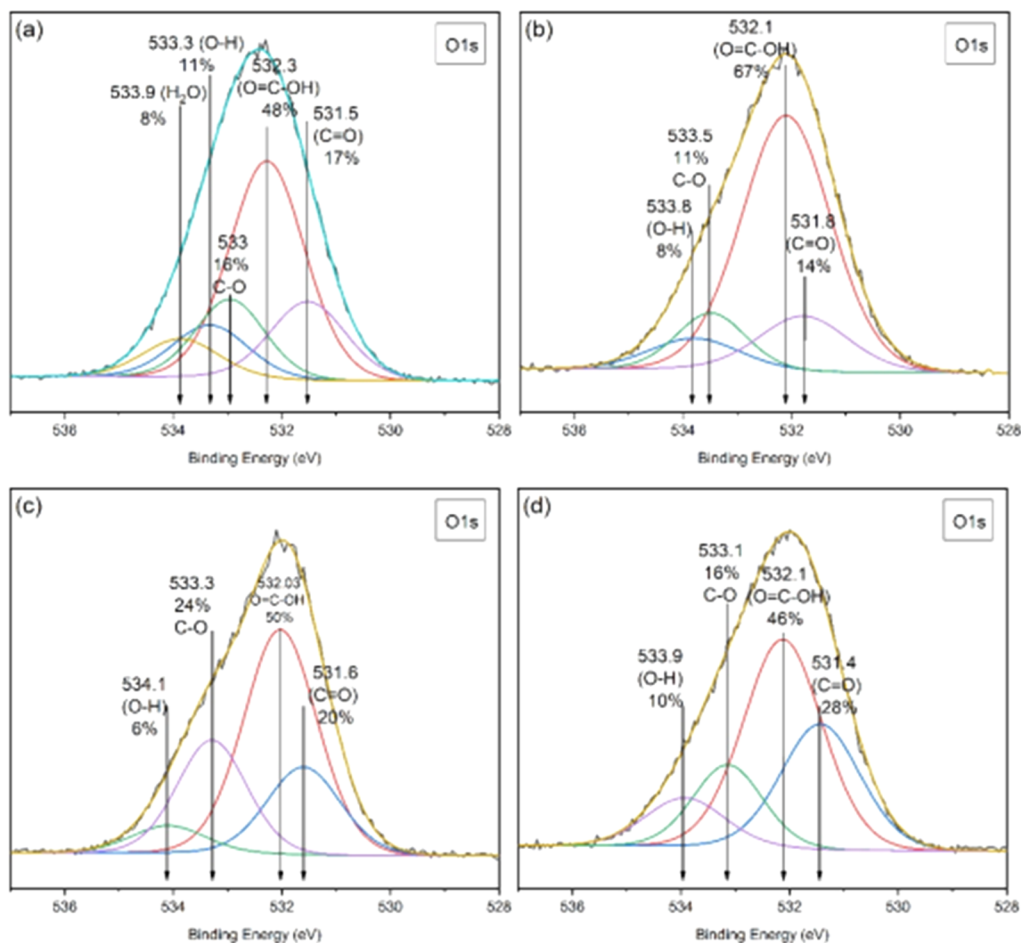


Figure 4. O 1s spectra of samples (a) C2-CDs, (b) C4-CDs, (c) T2-CDs, and (d) T4-CDs.

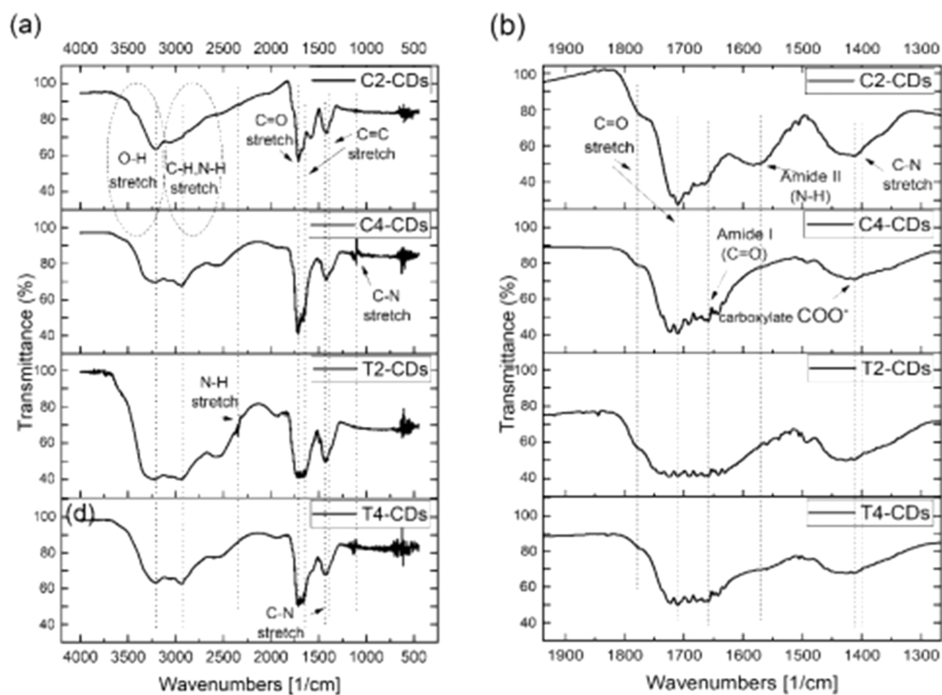


Figure 5. FT-IR spectra of samples C2-CDs, C4-CDs, T2-CDs, and T4-CD at (a) 500–4000 cm<sup>-1</sup>, (b) 1250–1950 cm<sup>-1</sup>.

the synthesis time. In addition, it can be seen from Figure 5a that, compared to C2-CDs, more amide groups are bonded to

the surface of C4-CDs because of the weakening of C=O stretching vibrations at 1708 cm<sup>-1</sup> due to carboxyl groups and

at  $1776\text{ cm}^{-1}$  due to imide groups, and the increase of  $\text{C}=\text{O}$  absorption band at  $1655\text{ cm}^{-1}$  due to amide groups.<sup>25,29</sup> Also, FT-IR spectra in Figure 5a,b illustrate that  $\text{C}=\text{O}$  bond oscillations at  $1650\text{--}1658\text{ cm}^{-1}$  and  $\text{C}-\text{N}$  bond at  $1232\text{ cm}^{-1}$  are increased for sample C4-CDs. The same behavior and increase of the  $\text{C}=\text{O}$  absorption band at  $1655\text{ cm}^{-1}$  due to amide groups were also observed for the FT-IR spectra of T2-CDs and T4-CDs. The chemical bonds of the CDs determined by FT-IR were in good agreement with XPS results.

UV-vis absorption spectra of all aqueous solutions of CDs exhibited shoulders at  $202\text{--}211\text{ nm}$ , which is assigned to the electron transitions from the  $\pi$  (or  $n$ ) orbital to the  $\pi^*$  orbital of the  $\text{C}=\text{C}$  bonds (Figure 6, inset). The absorption spectra of

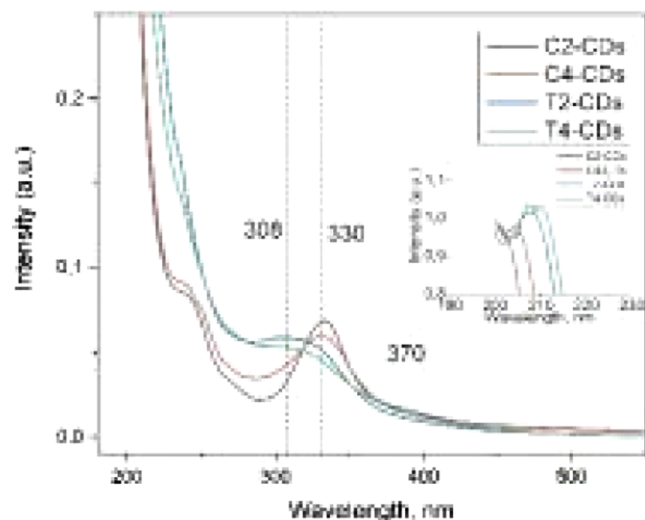


**Figure 6.** UV-vis absorption spectra of samples C2-CDs, C4-CDs, T2-CDs, and T4-CD. The inset shows absorption peaks with maxima at  $202\text{--}211\text{ nm}$ .

C2-CDs, C4-CDs, T2-CDs, and T4-CDs show the bands centered at  $332$ ,  $330$ ,  $308$ , and  $309\text{ nm}$ , respectively (Figure 6). According to previous studies, the peaks at  $308\text{--}309$  and  $330\text{--}332\text{ nm}$  correspond to surface states (in particular to carbonyl group  $\text{C}=\text{O}$ ).<sup>29,30</sup> Additionally, these spectra have an absorption edge extending to  $500\text{ nm}$ , which demonstrated the formation of nanocarbon.<sup>31</sup>

Figure 7 shows the PL emission spectra of the prepared CDs at excitation wavelengths  $300\text{--}500\text{ nm}$  with increments of  $20\text{ nm}$  (2D PL spectra are shown in Figure S3 (see Supporting Information, Figure S3)). The PL intensity of the emission wavelength of all CDs depends on the excitation wavelength. When the excitation wavelength was changed from  $300$  to  $320\text{ nm}$ , the PL intensity increased due to the transition of electrons from the  $n$  orbital to the  $\pi^*$  orbital of the graphitic bond cores.<sup>25</sup> This emission is highly intense, while the excitation in the far UV ( $\pi\text{--}\pi^*$  absorption band) returns very low PL.<sup>31</sup> Additionally, when the excitation wavelength increased from  $320$  to  $500\text{ nm}$ , the gradual decrease in the intensity of the emission peak was observed due to low optical absorption in the visible range. The maximum peaks of intensity were observed at  $432$ ,  $422$ ,  $417$ , and  $405\text{ nm}$  under the excitation of  $320\text{ nm}$  for C2-CDs, C4-CDs, T2-CDs, and T4-CDs, respectively. Accordingly, the PL emission of the CDs originated due to the radiative recombinations inside the carbon core and nitrogen moieties and (or) carbonyl functional groups present on the CD surface.<sup>25</sup> PL QY is

estimated to be  $51$ ,  $26.4$ ,  $47.2$ , and  $35.9\%$  for C2-CDs, C4-CDs, T2-CDs, and T4-CDs, respectively. Degradation of the PL spectra of the C2-CDs sample after synthesis and after 1 year is shown in Figure S4 (see Supporting Information, Figure S4). The PL degradation is related to the oxidation and aggregation of nanoparticles and the PL degradation behavior for other samples is similar. The lifetime of the fluorescence for all samples is  $9\text{--}10\text{ ns}$  at excitation  $300\text{ nm}$ . Time-resolved decay profiles are presented in Figure S5 (see Supporting Information, Figure S5).

## 4. DISCUSSION

The carbon cores of CDs are classified into two types depending on the degree of  $\text{sp}^2$  carbon hybridization: graphite crystalline and amorphous cores. It is known that only at temperatures above  $300\text{ }^\circ\text{C}$ , the graphitization of the core of CDs occurs. We assume that the core of the synthesized CDs has an amorphous structure because in our experiment, the synthesis temperature did not exceed  $220\text{ }^\circ\text{C}$ . However, TEM images of C4-CDs show lattice fringes, which are close to the  $(100)$  and  $(002)$  diffraction facets of graphite carbon. We consider that the formation of the graphite core in C4-CDs occurs because of long synthesis ( $4\text{ h}$ ) and high pressure in the autoclave.

The optical properties of CDs depend on their morphological structure and chemical composition. The PL of CDs has been mainly suggested to originate from the conjugated structures of the carbon core (or quantum confinement effect), the surface state of functional groups, and fluorescent molecules on the edges and surface of CDs.<sup>9</sup> In previous studies, the PL mechanism is usually explained by the synergistic effect between the conjugated  $\pi$ -domains of the carbon core and surface/edge state. The role of the structure of the core is obvious due to the fact that the undoped pure CDs have a radiation in the UV region from the core emission and doping of CDs with heteroatoms shifts the PL emission region to the red region.<sup>32</sup>

The role of surface states in the emission PL of CDs also introduces a significant contribution due to the fact that the behavior of emission is affected by changes in pH, oxidation level, solvatochromic effect, and passivation/functionalization of surface.<sup>20,21</sup> The presence of different nitrogen moieties provides stable surface energy traps, which participate in the PL emission.<sup>33</sup> Nitrogen moieties can tune the emission properties of CDs, specifically, was found that blue emissions refer to pyrrole nitrogen, green emissions to pyridine nitrogen, and red emissions to the distortion of *p*-phenylenediamine.

We proposed that the PL mechanism in our CDs was due to the fluorescent molecules on the edges and surface of CDs. Specifically, the main contribution to PL originated from molecules (or chemical groups), which are connected to the  $\text{sp}^2$  clusters. Reckmeier et al. synthesized two types of CDs: CDs from CA and ammonia by the hydrothermal method and CDs from CA and supercritical ammonia by the ammonothermal method.<sup>34</sup> By studying the optical and structural properties of these CDs, they concluded that the main contribution to the PL is carried by the fluorophores based on citrazinic acid derivatives (CADs), which formed during the synthesis. In particular, the presence in FT-IR results of peak  $\text{C}-\text{N}$  stretching at  $1400\text{--}1423\text{ cm}^{-1}$  can be attributed to the pyridone unit of the fluorophore based on CAD, also, the peaks of stretching vibrations  $\text{N}-\text{H}/\text{O}-\text{H}$  at  $3209\text{--}3309\text{ cm}^{-1}$ , amide I ( $\text{C}=\text{O}$ ) and amide II ( $\text{N}-\text{H}$ ) vibrations at

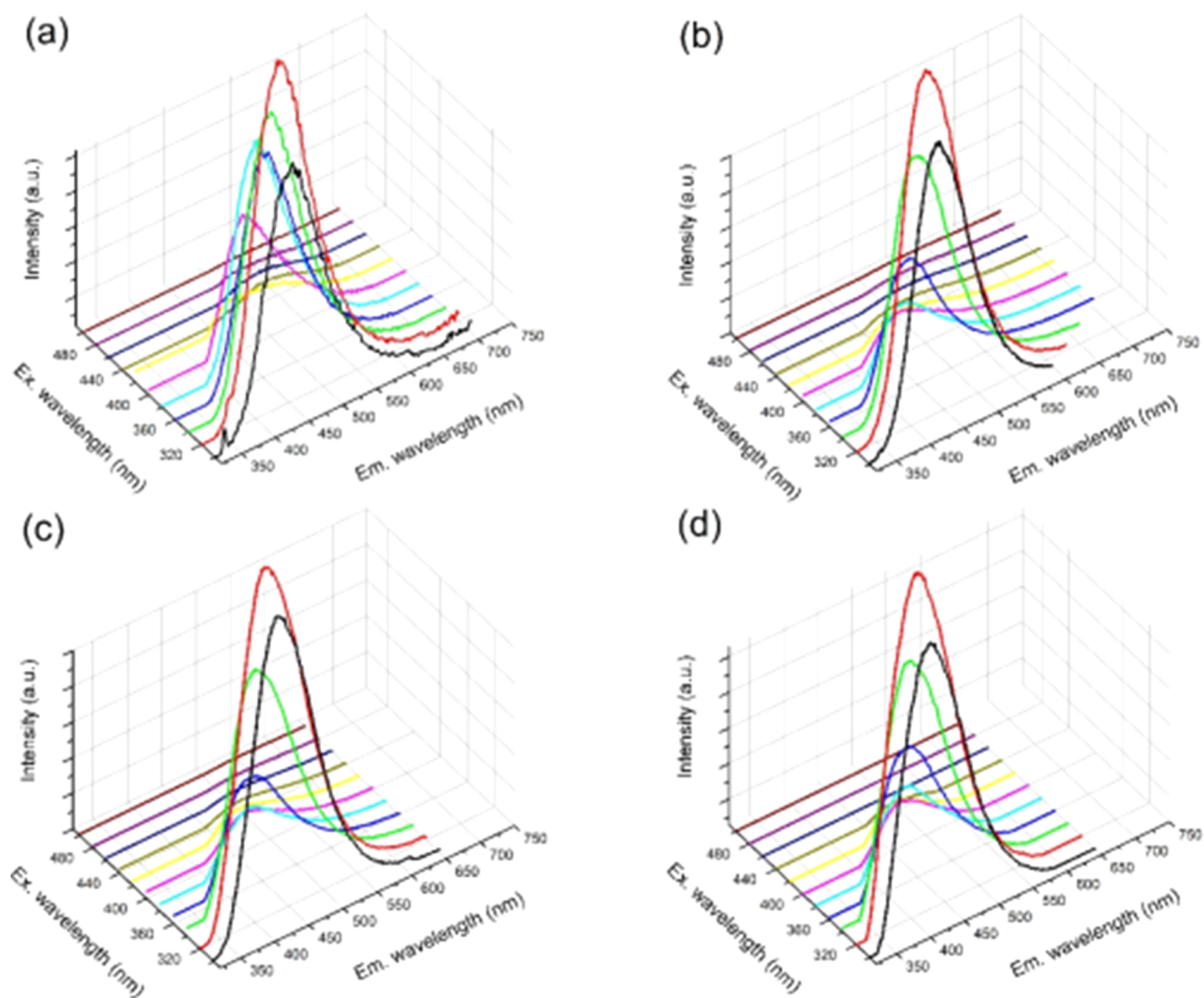


**Figure 7.** PL spectra of samples (a) C2-CDs, (b) C4-CDs, (c) T2-CDs, and (d) T4-CDs at excitations 300 (black), 320 (red), 340 (green), 360 (blue), 380 (cyan), 400 (pink), 420 (yellow), 440 (dark green), 460 (dark blue), 480 (purple), and 500 nm (dark red lines).

1650–1658  $\text{cm}^{-1}$  and 1553–1565  $\text{cm}^{-1}$ , and carboxylate  $\text{COO}^-$  vibration at 1420 indicated the ammonium salt of citrazinic acid (Figure 5b).<sup>34</sup>

Additionally, the presence of peaks  $\text{HO-C=O}$ ,  $\text{C-N-C}$ ,  $\text{C=O}$ , and  $\text{C-O}$  in our results of XPS confirms the formation of CAD at the edges and surface of CDs (Figures 2–5). In the C 1s spectra, the intensity of the  $\text{sp}^2$  and  $\text{sp}^3$  peaks increases with an increase in the synthesis time: the peak areas are 4 and 42% for C2-CDs, and the peak areas are 7.5 and 55.5% for C4-CDs, respectively (Figure 2a,b). These changes are consistent with the fact that the lateral size of the CD and density of defects on their surface increase with an increase in the synthesis time. The intensities of the  $\text{sp}^2$  and  $\text{sp}^3$  peaks of samples T2-CDs and T4-CDs have the similar behavior: the peak areas are 15 and 33% for T2-CDs, and the peak areas are 17 and 40% for T4-CDs, respectively (Figure 2c,d). The samples of CDs synthesized from TA have a higher percentage of  $\text{sp}^2$  hybridization and a lower percentage of  $\text{sp}^3$  hybridization in XPS C 1s spectra compared to samples synthesized from CA. We assume that the peculiarities of the chemical structure of TA increase  $\text{sp}^2$  hybridization rather than  $\text{sp}^3$  hybridization during synthesis.

Furthermore, we have found that the number of fluorophores based on CAD in CDs decreases with the increase in the lateral size of CDs due to aggregation. This fact is confirmed by the data of PL QY: 51 and 26.4% for C2-CDs and C4-CDs, and 47.2 and 35.9% for T2-CDs and T4-CDs, respectively. Reckmeier et al. explain the occurrence of aggregation by two reasons: (1) ammonium salts of citrazinic acid are hydrophilic in their carboxylate functionality and relatively hydrophobic at the aromatic unit, which gives the molecule a surfactant-like character and promotes its aggregation; (2) aggregation of fluorophore molecules is facilitated due to intermolecular hydrogen bonding and  $\pi$ - $\pi$  stacking of the pyridone unit.<sup>34</sup> High-resolution C 1s XPS spectra show in Figure 2 that the decrease of the C–N peak with the increase in synthesis time from 21 to 10% for C2-CDs and C4-CDs and from 19 to 14% for T2-CDs and T4-CDs probably indicates the aggregation of fluorophores based on CAD. Moreover, the changes in the FT-IR spectra of samples C4-CDs and T4-CDs relative to the  $-\text{OCNH}-$  linker, in particular, a decrease in amide II (N–H) bond at 1553–1565  $\text{cm}^{-1}$  with an increase of amide I (C=O) at 1650–1658  $\text{cm}^{-1}$ , can be associated with the aggregation of CAD due to increased synthesis time.

The main difference in the structure of CA and TA is that in TA the carbon chain has the “chair” type and the functional groups are on opposing sides of the carbon chain (the carbon chain in CA has the “zigzag” type). As viewed in Figure 1b, the T4-CDs are interconnected in the form of tree-like chains, this is similar to the chemical structure of dendrimers. The carbon core of T4-CDs can be thought of as the core of a dendrimer, and this core can be connected to the core of other carbon dots through branching of single molecules. We consider that they form a dendrimeric behavior due to molecular recognition (non-covalent bonding). We suppose that the aggregation of fluorophores in the case of sample T4-CDs is less intense because of the dendrimer-like structure. The  $sp^2$  peak increased from 15 to 17% in the C 1s spectra of T2-CDs and T4-CDs (Figure 2c,d), that is, the merger of carbon cores or their expansion was less intense compared to an increase of  $sp^2$  peak from 4 to 7.5% in samples C2-CDs and C4-CDs (Figure 2a,b); therefore, the PL QY of T4-CDs (35.9%) is higher than PL QY of C4-CDs (26.4%).

In addition to CAD, other isolated  $sp^2$  clusters should be formed in CDs, which contribute to the PL of CDs. In our early work, CDs without the nitrogen precursors were synthesized.<sup>13,35</sup> These CDs have a blue emission and the UV absorption spectrum only presents a shoulder at 300–310 nm. As the excitation wavelength increases from 300 to 500 nm, the PL intensity decreases gradually with the red-shifting of the emission spectrum. Probably, the PL contribution from isolated  $sp^2$  clusters can probably be summed with the PL contribution of CAD. However, PL QY of CDs is equal to only about 5%, which is considerably lower than that of CDs presented in this work. Therefore, CAD should play a more important role than isolated  $sp^2$  clusters on PL properties of CDs.

The absorption spectra of CDs synthesized from CA and TA showed one significant difference. The absorption peaks of C2-CDs and C4-CDs are shifted into the red region to 330–332 compared to T2-CDs and T4-CDs (308–309 nm) (Figure 6). According to the XPS N 1s results (Figure 3), the CDs from CA had more graphitic nitrogen, while the CDs from *trans*-aconitic acid had a more pyrrole nitrogen at the edges and surface. These features of the chemical structures of these CDs are the main reason for the difference in their absorption and PL spectra. Also, the increase in the absorption rate in the valley at 286 nm of C4-CDs sample and the decrease of the shoulder intensity at 308 nm of the sample may be due to the aggregation of CDs with an increase in the synthesis time of the CDs.<sup>36</sup> The absorption peaks around 202–211 nm were assigned to  $\pi-\pi^*$  transitions, arising from the conjugated  $\pi$  electrons in the aromatic rings of the CAD, and the peaks at 308–332 nm are assigned to  $n-\pi^*$  transitions. Reckmeier et al. argue that such an assignment does not hold up when aggregated aromatic structures are involved.<sup>34</sup> In this case,  $\pi-\pi^*$  transitions of intermolecular charge transfer contribute to the high energy part of the 308–332 nm peaks, while the aggregation-induced overlap of molecular orbital results in the formation of additional low energy states.<sup>34,37</sup>

As shown in Figure 7, all the four types of obtained CDs present high intensity PL with blue emission and exhibit similar PL properties. The maximum peak of the emission curve showed a slight dependence on the excitation wavelength in the range of 320–380 nm for all samples, suggesting that the luminescence originated from a molecular state.<sup>38</sup> Specifically, the peaks have values of 432, 422, 417, and 405 nm, for C2-

CDs, C4-CDs, T2-CDs, and T4-CDs at 320 nm excitation, respectively. At an excitation wavelength of 340 nm, the peaks shift to the red region and are observed at 442, 427, 420, and 417 nm for C2-CDs, C4-CDs, T2-CDs, and T4-CDs, respectively. At an excitation wavelength of 360, the maxima are also red-shifted and observed at 447, 434, 432, and 436 nm for C2-CDs, C4-CDs, T2-CDs, and T4-CDs, respectively. Additionally, the luminescence maximum peak for C4-CDs is shifted to the blue region by 10 nm and for T4-CDs by 12 nm with an increase in the synthesis time.

The following conclusions can be drawn about the influence of synthesis time on the optical properties of CDs: (1) the lateral size of CDs and the density of defects on their surface increase with the increase in synthesis time; (2) the number of CAD-based fluorophores in CDs decreases with the increase in synthesis time due to aggregation; and (3) the maximum PL QY was observed in the sample C2-CDs (51%), while the sample with longer synthesis time C4-CDs had only almost half the PL QY (26.4%) because of the aggregation of fluorescent molecules. Additionally, the luminescence peak maximum of C4-CDs and T4-CDs samples with long synthesis times shifts to the blue region by 10–12 nm, which also indicates a decrease in the contribution of CAD-based fluorescent molecules to the PL of CDs.

## 5. CONCLUSIONS

In summary, we have synthesized CDs with a high PL QY of 51% by hydrothermal treatment of CA and TA as the carbon source and ammonia solution as the N dopant. The main difference in CDs based on TA is the formation of CDs in a dendrimer-like structure, while CDs from CA are separately formed spherical nanoparticles. PL emission spectra of CDs show peaks at 409–435 nm with the maximum intensity at an excitation wavelength of 320 nm, which are usually attributed to  $\pi-\pi^*$  transitions of C=C bonds and  $n-\pi^*$  transitions of C=O bonds in CDs. Additionally, the dependence of the radiation wavelength on the excitation in PL spectra is observed. Our results of the structural and optical properties of CDs imply that molecular fluorophores are an important part of the structure; in particular, the main contribution to the PL is carried by the fluorophores based on CAD, which formed during the synthesis of CDs. The results of FT-IR and XPS spectroscopy confirm the presence of chemical bonds of citrazinic acid in CD structures. At the increase time of synthesis, the aggregation of CDs and the decrease of PL QY are observed. The CDs can be considered as hybrid particles in which the carbon core contains aggregated fluorophores or the aggregated fluorophores are located on the surface of the carbon core.

## ■ ASSOCIATED CONTENT

### SI Supporting Information

The Supporting Information is available free of charge at <https://pubs.acs.org/doi/10.1021/acsomega.2c05503>.

Size distributions; XPS-spectra; 2D PL spectra; emission decay curves of samples C2-CDs, C4-CDs, T2-CDs, and T4-CDs; and PL spectra degradation of sample C2-CDs (PDF)

## AUTHOR INFORMATION

## Corresponding Author

Aleksandra Tomskaya – A.M. Prokhorov General Physics Institute, RAS, Moscow 119991, Russia; Moscow Institute of Physics and Technology, Dolgoprudny 141701, Russia; North-Eastern Federal University, Yakutsk 670000, Russia; [orcid.org/0000-0001-9248-779X](https://orcid.org/0000-0001-9248-779X); Email: [ae.tomskaya@s-vfu.ru](mailto:ae.tomskaya@s-vfu.ru)

## Authors

Igor P. Asanov – Nikolaev Institute of Inorganic Chemistry SB RAS, Novosibirsk 630090, Russia

Irina Yushina – Nikolaev Institute of Inorganic Chemistry SB RAS, Novosibirsk 630090, Russia

Mariana I. Rakhmanova – Nikolaev Institute of Inorganic Chemistry SB RAS, Novosibirsk 630090, Russia

Svetlana Smagulova – North-Eastern Federal University, Yakutsk 670000, Russia

Complete contact information is available at:

<https://pubs.acs.org/10.1021/acsomega.2c05503>

## Notes

The authors declare no competing financial interest.

## ACKNOWLEDGMENTS

The authors are grateful to the Russian Science Foundation (project no. 20-42-08004), Ministry of Education and Science of Russia (FSRG 2020–0017), and Russian Foundation for Basic Research (project no. 20-32-90071) for financial support.

## REFERENCES

- (1) Li, L.; Zhao, W.; Luo, L.; Liu, X.; Bi, X.; Li, J.; Jiang, P.; You, T. Electrochemiluminescence of Carbon-Based Quantum Dots: Synthesis, Mechanism and Application in Heavy Metal Ions Detection. *Electroanalysis* **2022**, *34*, 608–622.
- (2) Wu, Z.; Li, W.; Chen, J.; Yu, C. A Graphene Quantum Dot-Based Method for the Highly Sensitive and Selective Fluorescence Turn on Detection of Biothiols. *Talanta* **2014**, *119*, 538–543.
- (3) Dong, Y.; Shao, J.; Chen, C.; Li, H.; Wang, R.; Chi, Y.; Lin, X.; Chen, G. Blue Luminescent Graphene Quantum Dots and Graphene Oxide Prepared by Tuning the Carbonization Degree of Citric Acid. *Carbon* **2012**, *50*, 4738–4743.
- (4) Li, H.; Yan, X.; Kong, D.; Jin, R.; Sun, C.; Du, D.; Lin, Y.; Lu, G. Recent Advances in Carbon Dots for Bioimaging Applications. *Nanoscale Horiz.* **2020**, *5*, 218–234.
- (5) Gao, F.; Ma, S.; Li, J.; Dai, K.; Xiao, X.; Zhao, D.; Gong, W. Rational Design of High Quality Citric Acid-Derived Carbon Dots by Selecting Efficient Chemical Structure Motifs. *Carbon* **2017**, *112*, 131–141.
- (6) Atchudan, R.; Chandra Kishore, S.; Gangadaran, P.; Jebakumar Immanuel Edison, T. N.; Perumal, S.; Rajendran, R. L.; Alagan, M.; Al-Rashed, S.; Ahn, B. C.; Lee, Y. R. Tunable Fluorescent Carbon Dots from Biowaste as Fluorescence Ink and Imaging Human Normal and Cancer Cells. *Environ. Res.* **2022**, *204*, 112365.
- (7) Atchudan, R.; Edison, T. N. J. I.; Perumal, S.; Muthuchamy, N.; Lee, Y. R. Hydrophilic Nitrogen-Doped Carbon Dots from Biowaste Using Dwarf Banana Peel for Environmental and Biological Applications. *Fuel* **2020**, *275*, 117821.
- (8) Nocito, G.; Calabrese, G.; Forte, S.; Petralia, S.; Puglisi, C.; Campolo, M.; Esposito, E.; Conoci, S. Carbon Dots as Promising Tools for Cancer Diagnosis and Therapy. *Cancers* **2021**, *13*, 1991.
- (9) Zuo, P.; Lu, X.; Sun, Z.; Guo, Y.; He, H. A Review on Synthesis, Properties, Characterization and Bioanalytical Applications of Fluorescent Carbon Dots. *Microchim. Acta* **2016**, *183*, 519–542.
- (10) Kasouni, A. I.; Chatzimitakos, T. G.; Troganis, A. N.; Stalikas, C. D. Citric Acid-Based Carbon Dots: From Revealing New Insights into Their Biological Properties to Demonstrating Their Enhanced Wound Healing Potential by in Vitro and in Vivo Experiments. *Mater. Today Commun.* **2021**, *26*, 102019.
- (11) Song, Y.; Zhu, S.; Zhang, S.; Fu, Y.; Wang, L.; Zhao, X.; Yang, B. Investigation from Chemical Structure to Photoluminescent Mechanism: A Type of Carbon Dots from the Pyrolysis of Citric Acid and an Amine. *J. Mater. Chem. C* **2015**, *3*, 5976–5984.
- (12) Lin, C.; Zhuang, Y.; Li, W.; Zhou, T. L.; Xie, R. J. Blue, Green, and Red Full-Color Ultralong Afterglow in Nitrogen-Doped Carbon Dots. *Nanoscale* **2019**, *11*, 6584–6590.
- (13) Tomskaya, A. E.; Prosvirin, I. P.; Egorova, M. N.; Smagulova, S. A.; Asanov, I. P. Structural and Optical Properties of N-Doped and B-Doped Carbon Dots. *J. Struct. Chem.* **2020**, *61*, 818–825.
- (14) Zhou, X.; Zhao, G.; Tan, X.; Qian, X.; Zhang, T.; Gui, J.; Yang, L.; Xie, X. Nitrogen-Doped Carbon Dots with High Quantum Yield for Colorimetric and Fluorometric Detection of Ferric Ions and in a Fluorescent Ink. *Microchim. Acta* **2019**, *186*, 67.
- (15) Meng, X.; Wang, Y.; Liu, X.; Wang, M.; Zhan, Y.; Liu, Y.; Zhu, W.; Zhang, W.; Shi, L.; Fang, X. Supramolecular Nanodots Derived from Citric Acid and Beta-Amines with High Quantum Yield and Sensitive Photoluminescence. *Opt. Mater.* **2018**, *77*, 48–54.
- (16) Yue, Z.; Economy, J. Carbonization and Activation for Production of Activated Carbon Fibers. *Activated Carbon Fiber and Textiles*; Elsevier, 2017.
- (17) Hu, S.; Trinchì, A.; Atkin, P.; Cole, I. Tunable Photoluminescence across the Entire Visible Spectrum from Carbon Dots Excited by White Light. *Angew. Chem., Int. Ed.* **2015**, *54*, 2970–2974.
- (18) Tian, X.; Yin, X. Carbon Dots, Unconventional Preparation Strategies, and Applications Beyond Photoluminescence. *Small* **2019**, *15*, 1901803.
- (19) Saleem, M.; Naz, M. Y.; Shukrullah, S.; Shujah, M. A.; Akhtar, M.; Ullah, S.; Ali, S. One pot sonochemical preparation of carbon dots, influence of process parameters and potential applications: a review. *Carbon Lett.* **2022**, *32*, 39–55.
- (20) Fu, M.; Ehrat, F.; Wang, Y.; Milowska, K. Z.; Reckmeier, C.; Rogach, A. L.; Stolarczyk, J. K.; Urban, A. S.; Feldmann, J. Carbon Dots: A Unique Fluorescent Cocktail of Polycyclic Aromatic Hydrocarbons. *Nano Lett.* **2015**, *15*, 6030–6035.
- (21) Liang, S.; Wang, M.; Gao, W.; Zhao, X. Effects of Elemental Doping, Acid Treatment, and Passivation on the Fluorescence Intensity and Emission Behavior of Yellow Fluorescence Carbon Dots. *Opt. Mater.* **2022**, *128*, 112471.
- (22) Wang, D.; Chen, M.; Wang, C.; Bai, J.; Zheng, J. Synthesis of Carbon Microspheres from Urea Formaldehyde Resin. *Mater. Lett.* **2011**, *65*, 1069–1072.
- (23) Krysmann, M. J.; Kellarakis, A.; Dallas, P.; Giannelis, E. P. Formation Mechanism of Carbogenic Nanoparticles with Dual Photoluminescence Emission. *J. Am. Chem. Soc.* **2012**, *134*, 747–750.
- (24) Dang, T. H. T.; Mai, V. T.; Le, Q. T.; Duong, N. H.; Mai, X. D. Post-Decorated Surface Fluorophores Enhance the Photoluminescence of Carbon Quantum Dots. *Chem. Phys.* **2019**, *527*, 110503.
- (25) Arul, V.; Sethuraman, M. G. Hydrothermally Green Synthesized Nitrogen-Doped Carbon Dots from Phyllanthus Emblica and Their Catalytic Ability in the Detoxification of Textile Effluents. *ACS Omega* **2019**, *4*, 3449–3457.
- (26) Liu, S.; Tian, J.; Wang, L.; Zhang, Y.; Qin, X.; Luo, Y.; Asiri, A. M.; Al-Youbi, A. O.; Sun, X. Hydrothermal Treatment of Grass: A Low-Cost, Green Route to Nitrogen-Doped, Carbon-Rich, Photoluminescent Polymer Nanodots as an Effective Fluorescent Sensing Platform for Label-Free Detection of Cu(II) Ions. *Adv. Mater.* **2012**, *24*, 2037–2041.
- (27) Xu, L.; Fang, G.; Pan, M.; Wang, X.; Wang, S. One-Pot Synthesis of Carbon Dots-Embedded Molecularly Imprinted Polymer for Specific Recognition of Sterigmatocystin in Grains. *Biosens. Bioelectron.* **2016**, *77*, 950–956.
- (28) Lu, W.; Gong, X.; Yang, Z.; Zhang, Y.; Hu, Q.; Shuang, S.; Dong, C.; Choi, M. M. F. High-Quality Water-Soluble Luminescent

Carbon Dots for Multicolor Patterning, Sensors, and Bioimaging. *RSC Adv.* **2015**, *5*, 16972.

(29) Han, X.; Zhong, S.; Pan, W.; Shen, W. A Simple Strategy for Synthesizing Highly Luminescent Carbon Nanodots and Application as Effective Down-Shifting Layers. *Nanotechnology* **2015**, *26*, 065402.

(30) Sudolská, M.; Otyepka, M. Exact Roles of Individual Chemical Forms of Nitrogen in the Photoluminescent Properties of Nitrogen-Doped Carbon Dots. *Appl. Mater. Today* **2017**, *7*, 190–200.

(31) Zhou, X.; Pan, Y.; Xu, J.; Wang, A.; Wu, S.; Shen, J. The Carbonization of Polyethyleneimine: Facile Fabrication of N-Doped Graphene Oxide and Graphene Quantum Dots. *RSC Adv.* **2015**, *5*, 105855–105861.

(32) Reckmeier, C. J.; Schneider, J.; Susha, A. S.; Rogach, A. L. Luminescent Colloidal Carbon Dots: Optical Properties and Effects of Doping [Invited]. *Opt. Express* **2016**, *24*, 312–340.

(33) Yuan, K.; Zhang, X.; Qin, R.; Ji, X.; Cheng, Y.; Li, L.; Yang, X.; Lu, Z.; Liu, H. Surface State Modulation of Red Emitting Carbon Dots for White Light-Emitting Diodes. *J. Mater. Chem. C* **2018**, *6*, 12631–12637.

(34) Reckmeier, C. J.; Schneider, J.; Xiong, Y.; Häusler, J.; Kasák, P.; Schnick, W.; Rogach, A. L. Aggregated Molecular Fluorophores in the Ammonothermal Synthesis of Carbon Dots. *Chem. Mater.* **2017**, *29*, 10352–10361.

(35) Tomskaya, A. E.; Egorova, M. N.; Kapitonov, A. N.; Nikolaev, D. V.; Popov, V. I.; Fedorov, A. L.; Smagulova, S. A. Synthesis of Luminescent N-Doped Carbon Dots by Hydrothermal Treatment. *Phys. Status Solidi B* **2018**, *255*, 1700222.

(36) Zhang, J.; Yang, L.; Yuan, Y.; Jiang, J.; Yu, S. H. One-Pot Gram-Scale Synthesis of Nitrogen and Sulfur Embedded Organic Dots with Distinctive Fluorescence Behaviors in Free and Aggregated States. *Chem. Mater.* **2016**, *28*, 4367–4374.

(37) Sudolská, M.; Dubecký, M.; Sarkar, S.; Reckmeier, C. J.; Zbořil, R.; Rogach, A. L.; Otyepka, M. Nature of Absorption Bands in Oxygen-Functionalized Graphitic Carbon Dots. *J. Phys. Chem. C* **2015**, *119*, 13369–13373.

(38) He, C.; Xu, P.; Zhang, X.; Long, W. The Synthetic Strategies, Photoluminescence Mechanisms and Promising Applications of Carbon Dots: Current State and Future Perspective. *Carbon* **2022**, *186*, 91–127.